PERGAMON

Mechatronics 14 (2004) 15–34

MECHATRONICS

Active damping within an advanced microlithography system using piezoelectric Smart Discs

Jan Holterman, Theo J.A. de Vries *

Control Laboratory, Faculty of Electrical Engineering, Drebbel Institute for Mechatronics, University of Twente, P.O. Box 217, 7500 AE Enschede, The Netherlands

Received 6 July 2001; accepted 19 December 2001

Abstract

Vibrations within high-precision machines are often badly damped, and may easily show up as a major factor in limiting the achievable accuracy. As it is hard to damp these vibrations by passive means, active vibration control may become inevitable within such machines. Robust active damping can be obtained by applying integral force feedback to so-called 'Smart Discs', i.e., active structural elements consisting of a piezoelectric position actuator and a collocated piezoelectric force sensor, which are inserted at appropriate locations within a machine frame.

A wafer stepper, i.e., the advanced microlithography system that is at the heart of integrated circuit manufacturing, is an excellent example of a high-precision machine with a frame that has low structural damping. Badly damped vibrations of the lens of the wafer stepper may in future limit the attainable line width of the circuit patterns. For this reason an active lens support, based on Smart Discs, is developed. Experiments with the active lens support show that the relative damping of the dominant vibration modes of the lens is increased from 0.2% to 16%, which effectively results in 86% reduction of the vibration amplitude.

Keywords: Active damping; Collocated control; Integral force feedback; High-precision machines; Microlithography

* Corresponding author. Tel.: +31-53-489-2783; fax: +31-53-489-2223.
E-mail address: mechatronics@rt.el.utwente.nl (T.J.A. de Vries).
URL: http://www.ce.utwente.nl/smartdisc.

0957-4158/$ - see front matter © 2003 Elsevier Ltd. All rights reserved.
doi:10.1016/S0957-4158(02)00093-4

1. Introduction

The design of high-precision machines heavily relies upon a limited number of well-known design principles, examples of which are *kinematic design*, *stiffness management*, *vibration isolation* and *thermal management* [1–5]. An issue that is equally important, but nevertheless often appears to be neglected in the design of a machine frame, is the realisation of sufficient *damping*. Especially within high-precision machines, damping values are very low. The lack of damping is an unwanted side-effect of the main design principle for achieving high accuracy, which states that uncertainty should be avoided as much as possible. For this reason, high-precision machine frames should be designed free of typical unpredictable damping phenomena like friction, hysteresis and micro-slip. As a consequence, vibrations within high-precision machines are often badly damped, and may easily show up as a major factor in limiting the achievable accuracy [6].

Due to the fact that damping is relatively hard to control by passive means, *damping management* is not yet a common issue in the design of high-precision machines. Instead, damping is usually realised in an ad hoc fashion, as an addition to an existing machine, e.g. by means of a tuned mass damper or via layers of highly dissipative material [1,2,4,7]. An important problem with this kind of damping solutions is the increased weight of the total structure. Furthermore, it is known that the smaller the vibrations are, the more difficult it is to damp them by such passive treatments [8,9]. It is for these reasons that, especially in the field of space and aircraft applications, active damping methods have gained a lot of research interest in the past decades [10,11]. As the accuracy demands for high-precision machines are continuously increasing, *active damping management* is becoming a necessary design principle for eliminating micro-vibrations, also within terrestrial applications.

At the Drebbel Institute for Mechatronics of the University of Twente, research is aimed at the development of an active structural element to be used within high-precision machines, in order to improve their dynamic behavior in general, with a particular focus on the damping properties. The active structural element, referred to as *Smart Disc*, consists of a piezoelectric position actuator collocated with a piezoelectric force sensor, and control and amplifier electronics [12,13]. Active damping by means of collocated actuator–sensor-pairs is a well-proven technique [8,11,14] and active damping elements have already shown their use as add-ons to vibrating structures [15–17]. However, a Smart Disc is envisioned as a load bearing structural element, rather than as an add-on. The idea of considering, already in the design phase, the utilization of load bearing active structural elements within high-precision machines, as such appears to be a new one.

An excellent example of a high-precision machine is the advanced microlithography system referred to as *wafer stepper*, that is at the heart of integrated circuit (IC) manufacturing. Microlithography is used by IC manufacturers to transfer a circuit pattern from a photomask to a thin slice of silicon referred to as the *wafer*, from which the ICs are cut out in the end. The circuit pattern is projected onto the wafer through a carefully constructed lens, which is in fact a complex system of lenses—see Fig. 1. The most important variable to control in the lithography process is the line

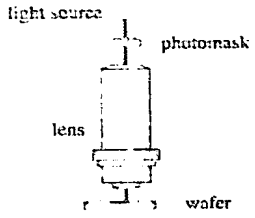

Fig. 1. Wafer stepper principle.

width of the circuitry on the wafer, as this width has direct impact on the final IC speed and performance [18]. The current IC line width is about 0.1 μm.

One of the possible future bottlenecks in decreasing the line width, and thus in the miniaturisation of ICs, is caused by badly damped micro-vibrations of the lens of the wafer stepper. Up till now, micro-vibration problems within high-precision machines could often be relieved by means of adequate isolation of the equipment from the floor, through which most of the disturbing vibrations enter. However, once the equipment is sufficiently isolated from floor vibrations, an other disturbance source becomes dominant: acoustics. It is practically impossible to come up with isolation means for acoustic vibrations, due to for instance the design principle concerning *thermal management* which requires a well-conditioned airflow within the machine. Damping of the lens vibrations by passive treatments has also turned out to be practically impossible. As a consequence, the wafer stepper constitutes a challenging test-bed for evaluation of the active damping potential of the Smart Disc concept. Experiments with prototype Smart Discs within the lens support of the wafer stepper are the subject of the present paper.

The paper is organised as follows. In Section 2, a close look is taken at the conventional lens support of the wafer stepper and at the vibrations constituting a major bottleneck in achieving the desired lithographic accuracy. In Section 3, the Smart Discs are introduced within a model of the lens support. Section 4 presents theory for robust, passivity based active vibration control. Section 5 deals with the design of a Smart Disc-based lens support and the way in which it passively affects the dynamic behavior of the wafer stepper lens. Section 6 subsequently describes the actual active damping experiments with the prototype Smart Discs within the lens support. Section 7 finally presents a discussion on the gathered experimental results.

2. Wafer stepper lens vibrations

2.1. Joystick modes

In this section we will take a closer look at the troublesome lens vibrations in the wafer stepper. Fig. 2 schematically depicts the parts of the wafer stepper that are

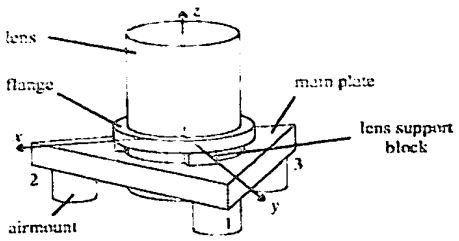

Fig. 2. Schematic view on wafer stepper.

important to us. Besides the lens, this figure shows the main plate, which serves as a positional reference for all other parts of the machine. The main plate is resiliently isolated from the floor, both passively and actively, by means of three so-called airmounts. The lens is held in a flange, which is connected to the main plate by means of three lens support blocks, only two of which are in sight in Fig. 2.

The lens support blocks are designed as much as possible according to kinematic design principles, in order to prevent the position of the lens being overconstrained. As a consequence, the overall stiffness of the lens suspension, and related resonance frequencies of the machine, cannot be increased infinitely. The two lowest vibration modes within the wafer stepper are referred to as the *joystick modes*. They correspond to tilt of the lens relative to the main plate, i.e., relative rotation of the lens around two perpendicular axes in the plane of mounting, where it should be noted that in Fig. 2 the choice for the x- and y-axis has been rather arbitrary (see Section 3.1). The joystick modes are mainly due to the limited vertical stiffness of the lens support blocks.

2.2. *Reference experiment*

A straightforward experiment on a specially modified wafer stepper set-up illustrates the small amount of damping in the machine. Focus here is on joystick-rotation around the x-axis in Fig. 2 (in-plane rotation in Fig. 3). The airmounts are

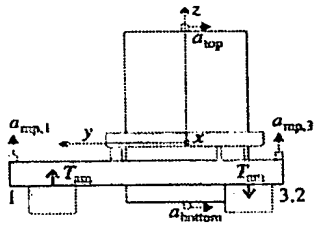

Fig. 3. Planar view on the set-up for illustration of joystick rotation around the x-axis.

used to apply a controllable torque T_{sm} around the x-axis of the main plate; we choose band-limited white noise of sufficient amplitude [19]. The relative tilt of the lens is reconstructed from appropriate acceleration measurements at both the main plate and the lens (indicated by the white cubes in Fig. 3). Here both the lens and the main plate are considered rigid. Obviously, the calculation of the relative tilt is only valid as long as the rigid-body assumption holds.

The experiment described above, serves as a reference for the Smart Disc experiments, as described in Sections 5 and 6. The results of the reference experiment are shown in Fig. 4:

- a time record of the calculated relative tilt (upper plot),
- the corresponding power spectral density (PSD) (see e.g. [20]; middle plot), and
- the corresponding cumulative PSD (lower plot).

The final value of the cumulative PSD is known to represent the power associated with the time-domain signal. In case the mean of the signal is equal to zero ($\mu = 0$), the square root of the power is equal to the standard deviation (σ) of the signal. As in case of a normally distributed signal, 99.7% of the values over time are within the range $[\mu - 3\sigma, \mu + 3\sigma]$, in this article we will use the so-called 3σ-value as a measure of the amplitude of the signal.

From the PSD plot, it can be seen that the calculated relative tilt is dominated by one of the joystick modes (which is known to be at 110 Hz). Note that the acceleration sensors also pick up a small contribution of the other joystick mode, at 105 Hz,

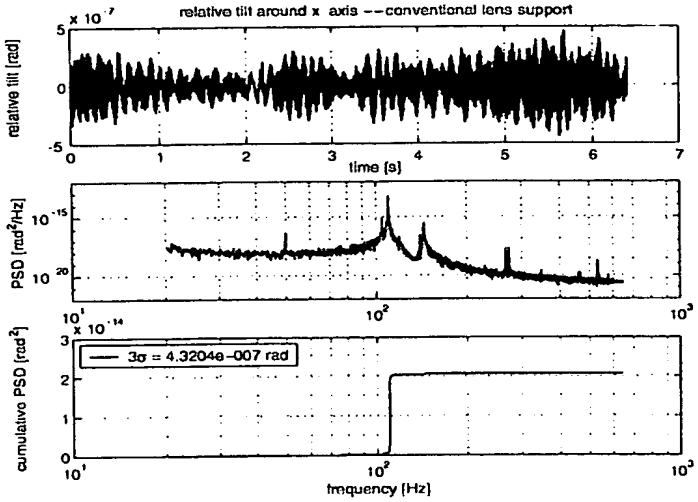

Fig. 4. Experimental results illustrating badly damped joystick modes.

indicating that the set-up is not perfectly symmetric. Other modes can be seen around 140 Hz (known to be due to internal bending of the main plate) and around 280 Hz (known to be so-called 'pendulum' modes, in which the lens moves horizontally with respect to the main plate in the plane of mounting).

From the lower plot in Fig. 4 the 3σ-value for the relative tilt appears to be 0.43 μrad, which is almost fully due to the lack of damping associated with the joystick mode at 110 Hz, as can be seen from the steep increment of the cumulative PSD. These experimental results unambiguously illustrate the need to damp the joystick modes, for instance by means of Smart Discs. To this end the next section deals with a model of the wafer stepper lens support and the way in which Smart Discs fit in.

3. Modelling Smart Discs within the lens support

3.1. Modelling a 'smart-supported' lens

In order to arrive at the simplest model describing the joystick modes, the main plate and the lens are regarded as rigid bodies. The compliance, which in practice is distributed throughout the whole machine, is lumped into the three lens support blocks, located symmetrically around a circular plane with radius r. The finite stiffness k_{LS} of each lens support block only permits local vertical movement of the lens relative to the main plate. The model that results as such describes the perpendicular joystick modes φ_x and φ_y as well as a third mode z_m, in which the lens moves vertically with respect to the main plate. The modes at 140 and 280 Hz, observed in the previous section, are not contained in this model.

Furthermore, assuming the resilient isolation to be perfect, which implies that the main plate is motionless despite the fact that the floor may be vibrating, Fig. 2 may be simplified to the *smart-supported lens* shown in Fig. 5a, where

- the single rigid body (m, J) accounts for both the inertia of the lens and the main plate,
- we have assumed pure rotational symmetry: the moment of inertia J is the same around any axis in the plane of mounting, i.e. the plane for which $z = 0$ in the model of Fig. 5a,
- the choice for (the modes around, respectively) the x- and the y-axes is, due to the assumed rotational symmetry, rather arbitrary,
- the three degrees of freedom z_1, z_2 and z_3 represent local relative vertical movements of the lens with respect to the main plate, and
- $F_{ext,i}$ denotes a generalised disturbance force, acting at the local coordinate z_i.

3.2. Modeling a 'smart' lens support block

Being the cause of the dominant vibration modes, the lens support blocks comprise the most appropriate locations to insert Smart Discs to actively damp these modes (as shown in Fig. 5a). The main parts of a Smart Disc (see Fig. 5b) are the position actuator z_{act} and the force sensor (indicated by F_{sens}). The actuator and

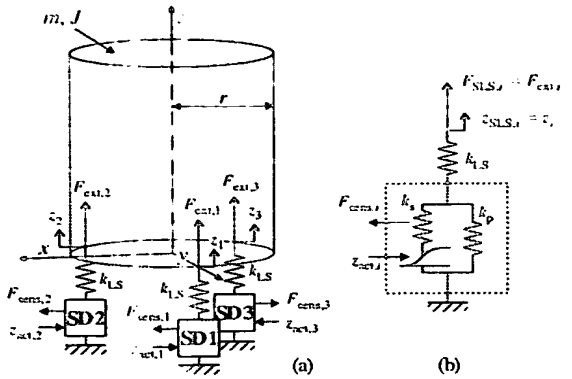

Fig. 5. (a) Smart-supported lens; (b) SLS block.

sensor together constitute an active element (so-called actuator–sensor-stack), the compliance of which is modeled by the single spring k_s. As this stack is to be made of piezoelectric material that should not be exposed to tensile forces, a preload element (k_p) is also taken into account in this model.

The active structural element that results after equipping a passive lens support block with a Smart Disc will be referred to as a *smart lens support* (SLS) *block*. It can conveniently be viewed as a two-port system with an *external* and an *internal* port. The variables at the external port are (see Fig. 5b).

- F_{SLS}, the *tensile* force present in the SLS block;
- z_{SLS}, the elongation of the SLS block;

whereas the variables at the internal port are

- F_{sens}, the *compressive* force present in the piezo stack, measured by the force sensor,
- z_{act}, the prescribed elongation of the piezo position actuator.

In the next section, we will take a look at the frequency responses associated to the simple model described above, so as to pave the way for Smart Disc-based active vibration control.

4. Active vibration control

4.1. Standard plant representation

Let us focus on active vibration control by means of Smart Disc 1 in Fig. 5. We will use the standard plant notation as shown in Fig. 6, with external (disturbance)

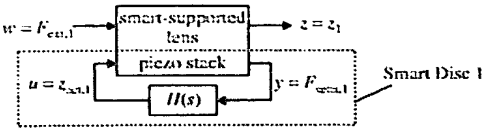

Fig. 6. Smart-supported lens in standard plant notation, with focus on Smart Disc 1.

input, $w = F_{ext,1}$, 'error' signal, $z = z_1$, control input, $u = z_{act,1}$, and measurement signal, $y = F_{sens,1}$. The frequency responses for this plant are shown in Fig. 7. Here the physical parameter values are taken from [19] (see Table 1) and the relative damping of the modes is set to 0.005, as a typical upper bound for the structural damping.

The upper left graph depicts the frequency response we are primarily interested in, $H^{z_1}_{F_{ext,1}}(j\omega)$, characterized by two vibration modes: one of the joystick modes (around the x-axis; at about 95 Hz, see Section 5.3) and the vertical vibration mode (at about 220 Hz). Note that, as a consequence of the perfect symmetry we assumed, the other joystick-mode (around the y-axis) is not excited by $F_{ext,1}$, and does not contribute to z_1.

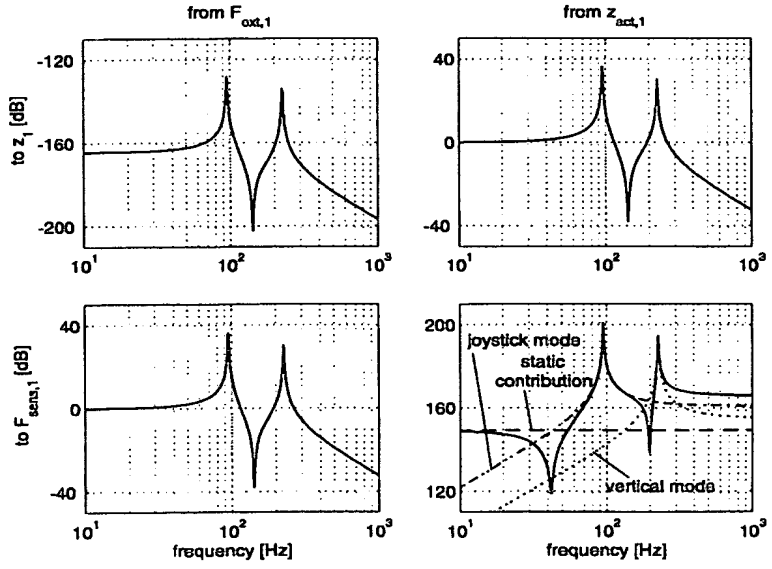

Fig. 7. Frequency responses for the system of Fig. 6.

Table 1
Parameter values for the model of the 'smart-supported' lens

Parameter	Value	Unit
r	0.225	m
m	250	kg
J	35.9	kg m^2
k_{1S}	1.75×10^8	N/m
k_s	4.8×10^9	N/m
k_p	2.9×10^7	N/m

It is well known that active damping can be robustly achieved by closing SISO control loops between *collocated* sensor–actuator-pairs, as the control law then inherently imposes a relation between two *power-conjugated* port variables [21]. This implies that the controller may easily be designed so as to extract energy from the system, i.e., effectively provide damping to the system. The robustness of such an active vibration control law, which in essence is a simple form of *passivity based control*, stems from the fact that it does not require detailed knowledge of the system [11].

4.2. Collocation: alternating pole-zero-pattern

The nice property of collocated actuator–sensor-pairs that enables robust active damping, can also be seen from the open loop frequency response $H_{z_{act,1}}^{F_{sens,1}}(j\omega)$, which for Smart Disc 1 in Fig. 7 is depicted in the lower right graph. Besides the contribution of the joystick mode φ_x his response exhibits a static contribution (due to the preload element in the Smart Disc) and the dynamic contribution of the translation mode. The preload contribution mainly manifests itself in the low-frequency range, which results in a non-zero lowest anti-resonance (at 40 Hz). The translation mode z_m contributes a second resonance (at 220 Hz), and an extra anti-resonance in-between the resonance peaks (at 200 Hz).

4.3. Integral force feedback [11,22]

The latter effect is typical for additional, unmodeled vibration modes in collocated transfer functions: in practice each vibration mode brings in a resonance and an anti-resonance, such that an *alternating* pole-zero-pattern results. A close look at this alternating pole-zero-pattern reveals that collocated actuator–sensor-pairs are indeed excellent for robust active vibration control, e.g. by use of *integral force feedback* (IFF) control in Fig. 6:

$$H(s) = H_{\mathrm{IFF}}(s) = \frac{K_{\mathrm{IFF}}}{s + p_{\mathrm{IFF}}} \tag{1}$$

The root locus of Fig. 8 shows the effect of closing the control loop with IFF, for a small value of p_{IFF}. Due to the alternating pole-zero pattern, in combination with the single controller pole close to the origin, for increasing K_{IFF} all poles are drawn into

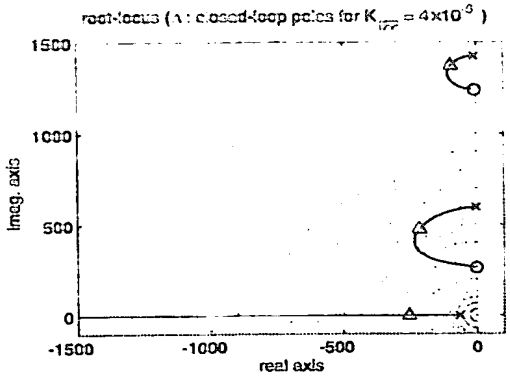

Fig. 8. Root locus for the IFF-controlled smart-supported lens; $H_{IFF}(s)H_{z,1}^{F_{ext,1}}(s)$.

the left half of the s-plane, which implies that all controllable resonances are damped. In this respect it should be noted that the maximum amount of modal damping that can be obtained by IFF largely depends on the level of modal controllability, which is determined by the distance between the poles and their corresponding zeros. It is easily seen that the closer a zero is to its corresponding pole, the smaller the attainable damping is for that particular mode [23,24].

The simplicity of the robust control law inherently leads to a slight problem, which is the *damping versus stiffness trade-off*: as the damping increases, the effective stiffness of the structure decreases. This can be seen from Fig. 9, which shows the

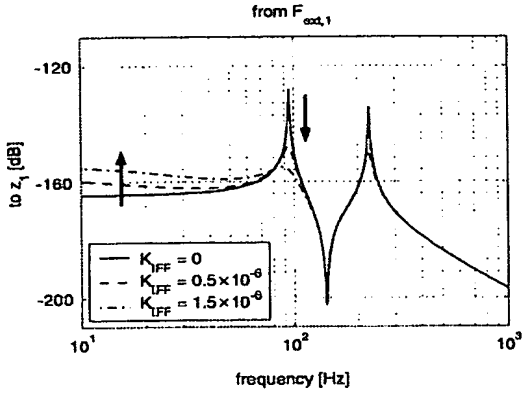

Fig. 9. Illustration of the damping-versus-stiffness trade-off within IFF.

frequency response of interest $H^{1}_{\text{Cm1}}(j\omega)$ for increasing values of the IFF-gain K_{IFF}. As a consequence, the ultimate control goal is not necessarily to maximize the damping for the joystick mode, but rather to optimize the relative rotation according to a certain well-chosen criterion.

For the active damping experiments on the wafer stepper lens support, however, IFF-tuning was performed manually on a trial-and-error basis. These experiments will be described in Section 6. The next section will first deal with the mechanical and electronic design of the SLS, and the differences between a conventionally and a 'smart but *passively* supported' wafer stepper lens, in terms of the dynamic behavior.

5. Smart lens support—design and passive behavior

5.1. Mechanical design

Having provided a theoretical setting for Smart Disc-based active damping within the wafer stepper lens support in the previous sections, in the sequel we will focus on practical issues, starting with the *mechanical design* of the SLS (Fig. 10). Here the main consideration has been to end up with a SLS block that is, in terms of its outer dimensions, a one-to-one replacement of the original lens support block. This facilitates a fair comparison between the dynamic behavior of the conventionally supported lens and the 'smart-supported' lens.

5.1.1. Piezoelectric stacks

For reasons of symmetry the SLS block has been equipped with *two* piezoelectric stacks (05 in Fig. 10; dimensions, 10 × 10 × 7.3 mm), the upper and lower faces of which have been glued to the steel frame of the SLS block (01 in Fig. 10). Both stacks consist of a multi-layer piezoceramic actuator (thickness, 4 mm; maximum stroke, 4 μm@100 V) and a single-layer piezoceramic sensor (thickness, 1 mm; sensitivity, 450 pC/N). Both actuators as well as both sensors are electrically connected in parallel, i.e., the two stacks together provide the functionality of a single Smart Disc.

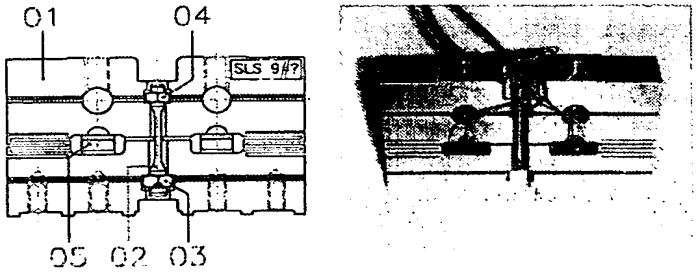

Fig. 10. SLS block—mechanical design.

5.1.2. Preload elements

Two preload elements have been designed. A bolt (02 in Fig. 10), with two accompanying nuts (03 and 04 in Fig. 10), provides the *functional preload* for the piezoelectric stacks; i.e. the bolt acts as the real preload element during operation of the SLS. From a safety point of view, additional preload measures have been taken: the 'accordion springs', i.e, the parallel flexure blades at both sides of the steel frame provide a small compressive preload force in case of absence of the preload bolt.

5.2. Electronic design

The SLS block described above is not a 'true' Smart Disc, as the amplifier and controller electronics were in separate boxes rather than miniaturised and integrated in the mechanical design. With respect to the electronics, the following remarks should be made. For a schematic overview of all electronics used, refer Fig. 11.

5.2.1. Actuator amplifier

Piezoelectric materials are characterized by a direct, nearly linear relationship between the deformation of the material and the charge built up in the material. Piezoelectric *ceramics*, however, are known to suffer from a considerable amount of hysteresis in the charge–voltage-characteristic. As a consequence, the voltage–displacement-characteristic also suffers from hysteresis. In order to circumvent this hysteresis, a *charge-feedback* amplifier is used for controlling the charge, q_{act}, rather than the voltage at the Smart Disc piezoelectric actuator [25].

Furthermore, the piezoelectric actuator is shunted with a resistance, in order to prevent drift of the actuator charge. As a consequence, the actuator is effectively charge-controlled only above the cut-off frequency (0.04 Hz) of the high-pass filter constituted by the capacitance of the piezoelectric actuator and the shunt resistance.

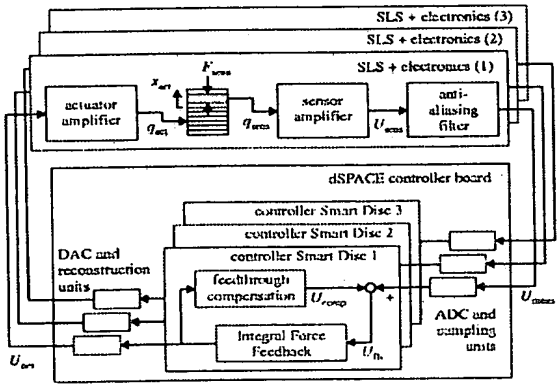

Fig. 11. Schematic overview of controller and amplifier electronics for the Smart Discs.

5.2.2. Sensor amplifier

Analogously to the actuator, drift of the charge at Smart Disc piezoelectric sensor has to be prevented. Therefore, the sensor has been shunted with an RC-circuit, yielding a highpass-filter with an appropriate cut-off frequency (0.1 Hz). For frequencies above the cut-off frequency, the capacitance of the RC-circuit effectively converts the sensor-charge q_{sens} to a voltage U_{sens}, which is subsequently fed to an amplifier. It would have been better however to use a true charge amplifier [26].

5.2.3. Control electronics

Though the intended SISO IFF-controllers for the Smart Discs are simple low-pass filters (Eq. (1)), which may easily be implemented using analog electronics, all processing for control has been performed by a dSPACE single-board controller, with a sampling frequency of 10 kHz. In order to prevent anti-aliasing, the electronic circuits for the sensors have been equipped with a fourth-order Butterworth low-pass filter, with a cut-off frequency of 2 kHz.

5.3. Experiment with passive smart lens support blocks

In order to examine the effect of the insertion of the passive, i.e., uncontrolled, SLS blocks on the dynamic behavior of the lens, a similar experiment as described in Section 2 has been performed.

5.3.1. Passive SLS block stiffness

Comparison of the experimental results (Fig. 12) with the original situation reveals that the stiffness of the lens support has decreased considerably, which can be explained from the fact that a solid slice of steel in a lens support block has been replaced by two piezoelectric stacks. Closer inspection of the dominant resonances leads to the following observations concerning the stiffness of the lens support, based on the fact that the resonance frequency of a vibration mode depends linearly on the square root of the effective stiffness involved.

- The resonance frequencies of the joystick modes have lowered from 110 to 95 Hz, indicating a decrease of the vertical stiffness of the lens support blocks. As the inertia of the set-up has not changed, the effective stiffness involved in the joystick modes has lowered to $(95/110)^2 \approx 0.75$ of the original level.
- The mode at 140 Hz (main plate bending) is hardly affected, as might be expected because the stiffness of the lens support is not involved in this mode.
- The resonance frequency of the pendulum modes has lowered from 280 to 180 Hz. This can be explained by a large decrease of the horizontal shear stiffness of the lens support blocks. The effective horizontal shear stiffness of the lens support has lowered to $(180/280)^2 \approx 0.50$ of the original level.

5.3.2. Passive SLS block damping

Despite the fact that the overall stiffness of the lens support has decreased considerably, Fig. 12 reveals that the 3σ-value did not increase. Instead, the 3σ-value

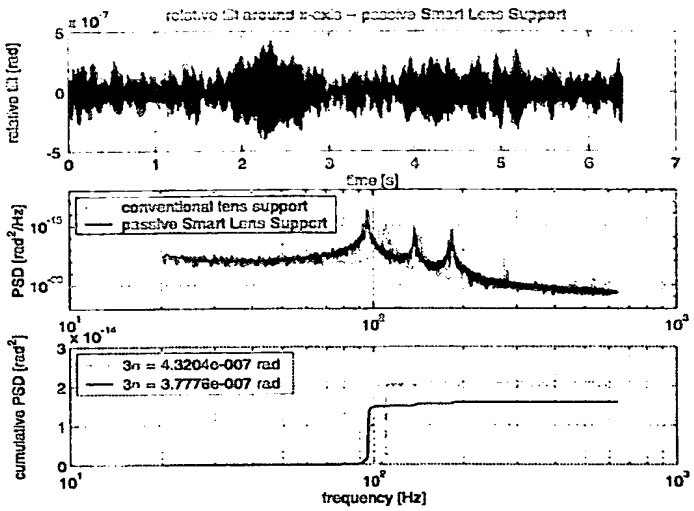

Fig. 12. Experimental results illustrating the effect of passive SLS blocks.

decreased from 0.43 to 0.38 μrad. This can be explained by an increase of the passive damping; additional experiments revealed that the relative damping involved in the joystick modes had increased from 0.2% to 0.5% [19]. The damping increase is due to a combination of hysteresis in the piezoelectric material, the resistive shunts for the piezos, and the viscoelasticity of the glue in the SLS block assembly.

From the cumulative PSD plot, however, it can be seen that the contribution of the joystick modes to the total relative tilt of the lens is still characterized by a steep increment, which underlines the introductory statement that active damping is becoming a necessity in high-precision machines. The next section deals with active damping experiments within the lens support of the wafer stepper.

6. Smart lens support—active damping experiments

6.1. Cross-contraction

In this section we will investigate to what extent the smart-supported lens behaves in accordance with the theoretical setting of Sections 3 and 4, and whether the joystick modes of the lens can indeed be damped accordingly.

As a start, in order to verify whether the SLS blocks have been correctly designed, the collocated and non-collocated Smart Disc frequency responses have been measured (i.e., the transfer from $U_{act,i}$ to $U_{meas,i}$, see Fig. 11). Due to the symmetry in the

set-up, all (three) collocated frequency responses as well as all (six) non-collocated frequency responses were quite similar [19]. Furthermore both the collocated and the non-collocated responses show the same resonance peaks. The particular alternating pole-zero-pattern indeed is observed in the collocated frequency responses (Fig. 13, left)

$$H_{\text{coll}}(j\omega) = \frac{U_{\text{meas},i}}{U_{\text{act},i}}(j\omega)$$

and *not* in the non-collocated frequency responses (Fig. 13, right)

$$H_{\text{non-coll}}(j\omega) = \frac{U_{\text{meas},j}}{U_{\text{act},i}}(j\omega) \quad i \neq j.$$

The alternating pole-zero-pattern can conveniently be seen from the phase plot, which for the collocated case varies between 0° and 180° (the gradual phase shift for increasing frequency is due to the anti-aliasing filter in the Smart Disc sensor electronics).

Closer inspection of the collocated frequency response however reveals that the pole-zero pattern is not as expected: each resonance is *followed instead of preceded* by an anti-resonance. This unexpected result can only be explained by a large negative

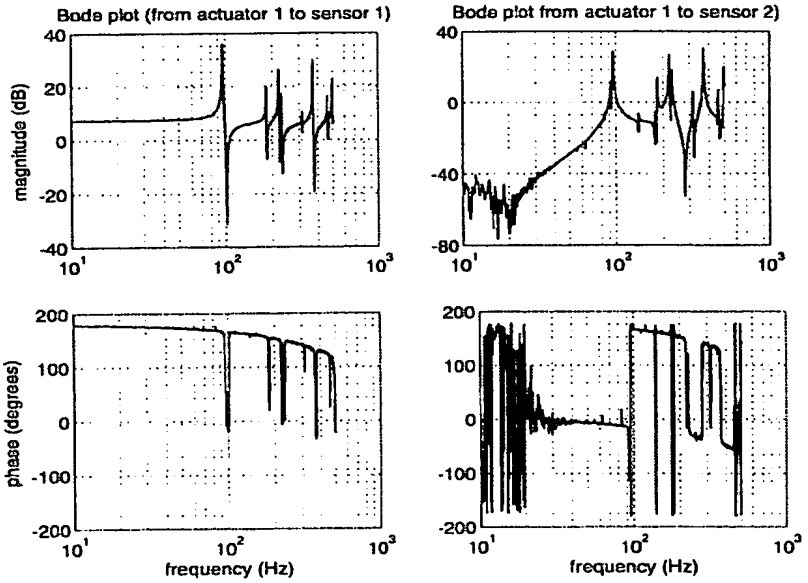

Fig. 13. Collocated (left) and non-collocated (right) frequency response.

static feedthrough term, whereas a small positive static feedthrough term was expected, because of the presence of the preload element [23]. Note that here the term 'static' refers to frequencies well below the resonance frequencies, rather than to a frequency of 0 Hz. The large negative static feedthrough term, in turn, can physically be explained as *cross-contraction* within the piezoelectric stacks. Instead of quasi-static compression of the sensor in vertical direction, cross-contraction of the total stack (as the actuator expands) results in an elongation of the sensor also, as the sensor is fixed tightly to the actuator. This problem could have been prevented by a better mechanical design [23].

6.2. Controller design

In order to be able to apply IFF to the SLS as described above, the pole-zero-pattern should be 're-flipped'. Furthermore, for observability and controllability reasons, the zeros should not only be re-flipped, but they should also be placed sufficiently far from the poles [24]. In other words, before applying IFF, the negative static feedthrough term should be compensated for appropriately. Though the resulting control law is not passive anymore, stability robustness is not endangered in practice, as long as 'overcompensation' is prevented [23].

The scheme according to which the static feedthrough compensation has been implemented is shown in Fig. 11. Here it is assumed that for low frequencies, the measured output depends linearly on the actuated input: $U_{\text{meas}} = c_{\text{lf}} U_{\text{act}}$. An estimate $U_{\text{comp}} = \hat{c}_{\text{lf}} U_{\text{act}}$ of the static contribution is subtracted from the measured signal U_{meas}, yielding the new feedback signal U_{fb} as input for the IFF-controller. A measurement of the compensated frequency response

$$H_{\text{comp}}(j\omega) = H_{\text{coll}}(j\omega) - \hat{c}_{\text{lf}},$$

with $\hat{c}_{\text{lf}} = -2.45$, is shown in Fig. 14.

Note that here no anti-resonance can be seen clearly in the magnitude plot; however, from frequency to frequency, the phase does increase to 180° as expected, be it very slowly and not via a sharp edge. Physically this implies that effectively, in-between the poles, there are still zeros, the locations of which, however, cannot be determined unambiguously. This in turn is caused by the fact that the frequency response from actuator input to sensor output suffers from hysteresis in both the actuator and the sensor, despite the fact that care is taken to circumvent this via the electronics (Section 5.2). Linear compensation thus as a matter of fact is not the best thing to do, but it is most easy, and for our experiments linear compensation turned out to be good enough.

The IFF controller has been tuned manually, as follows. First an appropriate value for the IFF pole has been chosen. With this value the IFF gain was gradually increased, in order to achieve maximum damping. The limiting factor here was instability of higher order modes due to non-ideal electronics characteristics (the gradual phase lag in Fig. 13), and not yet the fact that the low-frequency contribution started to dominate the 3σ-value [19]. The IFF controller settings thus ob-

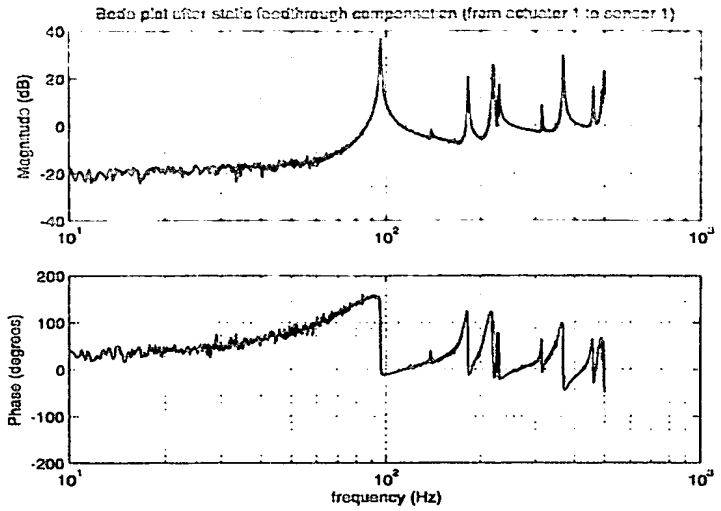

Fig. 14. Collocated frequency response after static feedthrough compensation.

tained are given by (with static feedthrough compensation as described above; see Fig. 11):

$$H_{\mathrm{IFF}}(s) = \frac{800}{s+87}$$

It should be noted that for the active damping experiments on the wafer stepper lens support, this controller setting has been used *for all three SLS blocks.*

6.3. Active damping results

In order to evaluate the active damping performance, the same experiments were performed as described in Sections 2 and 5. The results are given in Fig. 15. From the PSD plot (middle) the qualitative conclusion can be drawn that the joystick mode resonance peak is damped excellently, as it has nearly vanished. From the cumulative PSD plot (lower) we can draw quantitative conclusions.

Considered over the entire frequency range, the 3σ-value has decreased from (original) 0.43 μrad (100%), via (passive SLS) 0.38 μrad (12% reduction), to (active SLS) 0.10 μrad (77% reduction): an improvement of about a factor 4. However, we should bear in mind that the 3σ-calculation has been based on rigid-body assumptions, while the considerable contribution at 140 Hz is known to be due to internal main plate bending. As such the value 0.10 μrad is overestimated—note that this also holds for the original 0.43 μrad. When we concentrate purely on the contribution of

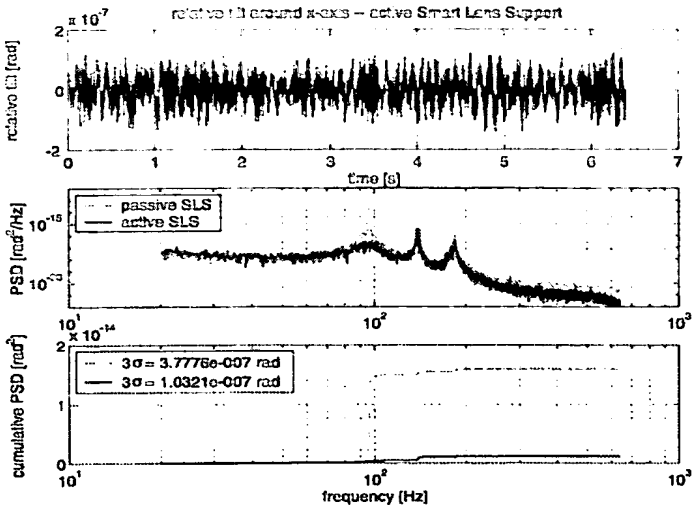

Fig. 15. Active damping results.

the joystick mode to the final 3σ-value, we see an improvement from (original) 0.43 μrad (100%), via (passive SLS) 0.37 μrad (14% reduction), to (active SLS) 0.06 μrad (86% reduction): an improvement of about a factor 7.

The relative damping that is associated with the joystick modes for the various situations, has also been determined from the various PSD plots. It has increased from (original) 0.2%, via (passive SLS) 0.5%, to (active SLS) 16%: an improvement of a factor 80 [19].

7. Conclusion

Prototype Smart Discs have been implemented successfully in an experimental set-up based on the lens support of a wafer stepper. Experiments with this set-up have shown the active damping potential of the Smart Disc concept in an industrial high-precision machine. With respect to the final accuracy of the wafer stepper, it is hard to correctly interpret the experimental results. Measurements have shown that Smart Disc-based active damping has reduced the amplitude of the dominant vibration modes (joystick modes at 100 Hz) by 86%, i.e., a factor 7 improvement. The relative damping of these modes even increased with a factor 80, from 0.2% to 16%.

Due to the fact that the Smart Disc concept is based on collocated actuator–sensor-pairs, active damping can be obtained with IFF control, which is a simple form of passivity based control, guaranteeing robustness with respect to both per-

formance and stability. However, a negative consequence of IFF, being a simple and robust control scheme, is the inherent damping versus stiffness trade-off. Furthermore, the theoretical stability robustness is in practice endangered by limitations of the sensor, the actuator, and the associated electronics.

A slight drawback of the insertion of the Smart Discs, is the lowered effective stiffness of the lens support. For the controllable modes the actively increased damping largely outweighs the stiffness loss. The resonance frequency of the uncontrollable pendulum modes however has decreased significantly (from 280 to 180 Hz). These modes thus have become more dominant, which negatively affects the overall machine accuracy. Current research aims at the design of a SLS block, such that the pendulum modes can also be controlled, i.e., damped actively.

An other problem that showed up in practice was negative static feedthrough from actuator to sensor, due to cross-contraction of the piezoelectric material. For the experiments, in order to apply IFF-control, the static feedthrough was compensated for linearly. The compensation in turn revealed that the hysteresis, known to be present in piezoelectric material, was not compensated for sufficiently by means of the amplifier electronics used. Current research aims at the design of Smart Discs such that negative static feedthrough is minimized.

Acknowledgements

We would like to thank *Bauke Tacoma*, *Bastiaan Jansen* and *Marcel Schwirtz* for their contribution to the Smart Lens Support experiments, and *Rien Koster* and *Johannes van Dijk* for their contribution throughout the entire Smart Disc project. Furthermore, we gratefully acknowledge *Frank Auer* for enabling us to perform Smart Disc experiments on the wafer stepper test-bed, and the *IOP Precision Technology* of the Dutch Ministry of Economic Affairs for financially supporting this research.

References

[1] Slocum AH. Precision machine design. Englewood Cliffs, NJ, USA: Prentice Hall; 1992.
[2] Smith ST, Chetwynd DG. Foundations of ultraprecision mechanism design. Philadelphia, PA, USA: Gordon and Breach Science Publishers; 1992.
[3] Nakazawa H. Principles of precision engineering. Oxford, UK: Oxford Science Publications; 1994.
[4] Hale LC. Principles and techniques for designing precision machines. PhD thesis, Massachusetts Institute of Technology, Cambridge, MA, USA; 1999.
[5] Koster MP. Constructieprincipes voor het nauwkeurig bewegen en positioneren. Enschede, The Netherlands: Twente University Press; 2000.
[6] Van Schothorst G. Active vibration control with piezoelectric Smart Discs. In: Conference proceedings SPIE smart structures and materials: mathematics and control in smart structures, vol. 3667. Newport Beach, California, USA March 1–5; 1999. p. 637–48.
[7] Rivin EI. Stiffness and damping in mechanical design. New York, USA: Marcel Dekker; 1999.
[8] Fanson JL, Anderson EH, Rapp D. Active structures for use in precision control of large optical systems. Opt Eng 1990;29(11):1320–7.

[9] Mead DJ. Passive vibration control. Chichester, UK: John Wiley & Sons; 1998.
[10] Joshi SM. Control of large flexible space structures. Berlin, Germany: Springer-Verlag; 1989.
[11] Preumont A. Vibration control of active structures, an introduction. Dordrecht, The Netherlands: Kluwer Academic Publishers; 1997.
[12] Holterman J, De Vries TJA, Koster MP. Experiment to evaluate the feasibility of the Smart Disc concept. In: Conference proceedings 6th UK mechatronics forum international conference, mechatronics 98. Skövde, Sweden, September 9–11; 1998. p. 217–22.
[13] Holterman J, De Vries TJA. Active structural elements within a general vibration control framework. In: Conference proceedings 1st IFAC conference on mechatronic systems, mechatronics 2000, Darmstadt, Germany, September 18–20; 2000. p. 997–1002.
[14] Anderson EH, Moore DM, Fanson JL, Ealey MA. Development of an active truss element for control of active structures. Opt Eng 1990;29(11):1333–41.
[15] Bronowicki AJ, Innis JW, Casteel S, Dvorsky G, Alvarez OS, Rohleen E. Active vibration suppression using modular elements. In: Conference proceedings SPIE smart structures and materials: smart structures and intelligent systems, vol. 2190; 1994. p. 717–28.
[16] Anderson EH, Holcomb MD, Bogue AX, Russo FM. Integrated electro-mechanical devices for active control of vibration and sound. In: Adaptive structures and materials systems symposium, international mechanical engineering congress and exposition, Dallas, Texas, USA; 1997.
[17] Spangler RL, Russo FM, Palombo DA. A compact integrated vibration control package. In: Conference proceedings SPIE smart structures and materials: smart structures and integrated systems, vol. 3041; 1997. p. 728–40.
[18] Edgar TF, Butler SW, Campbell WJ, Pfeiffer C, Bode C, Hwang SB, et al. Automatic control in microelectronics manufacturing: practices, challenges, and possibilities. Automatica 2000;36(11):1567–603.
[19] Jansen BSH. Smart Disc tuning and application. Enschede, Control Laboratory, Faculty of Electrical Engineering, University of Twente, M.Sc. thesis, Report no. 016R2000, 2000.
[20] Harris CM. Shock and vibration handbook. New York, USA: McGraw-Hill; 1996.
[21] Stramigioli S, Maschke B, Van der Schaft A. Passive output feedback and port interconnection. In: Conference proceedings 4th IFAC nonlinear control systems design symposium, Nolcos 98, Enschede, The Netherlands, July 1–3; 1998.
[22] Preumont A, Dufour JP, Malékian C. Active damping by a local force feedback with piezoelectric actuators. J Guidance, Contr Dynam 1992;20(2):390–5.
[23] Holterman J. Vibration control of high-precision machines with active structural elements. PhD thesis, Drebbel Institute for Mechatronics, University of Twente, Enschede, The Netherlands; 2002.
[24] Holterman J, De Vries TJA. Active and passive damping based on piezoelectric elements, Controllability issues. In: Conference proceedings 3rd workshop on European scientific and industrial collaboration, WESIC 2001. Enschede, The Netherlands, June 27–9; 2001. p. 179–88.
[25] Main JA, Garcia E, Newton DV. Precision control of piezoelectric actuators using charge feedback. J Guidance, Contr Dynam 1995;18(5):1068–73.
[26] Tichy J, Gautschi GH. Piezoelektrische Messtechnik: physikalische Grundlagen; Kraft, Druck- und Beschleunigungsaufnehmer; Verstärker. New York, USA: Springer Verlag; 1980.